

Spectroscopy and Photochemistry; General Theory

Hot Carrier and Surface Recombination Dynamics in Layered InSe Crystals

Chengmei Zhong, Vinod K. Sangwan, Joohoon Kang, Jan Luxa, Zdeněk Sofer, Mark C Hersam, and Emily A. Weiss

J. Phys. Chem. Lett., **Just Accepted Manuscript** • DOI: 10.1021/acs.jpcllett.8b03543 • Publication Date (Web): 14 Jan 2019

Downloaded from <http://pubs.acs.org> on January 15, 2019

Just Accepted

“Just Accepted” manuscripts have been peer-reviewed and accepted for publication. They are posted online prior to technical editing, formatting for publication and author proofing. The American Chemical Society provides “Just Accepted” as a service to the research community to expedite the dissemination of scientific material as soon as possible after acceptance. “Just Accepted” manuscripts appear in full in PDF format accompanied by an HTML abstract. “Just Accepted” manuscripts have been fully peer reviewed, but should not be considered the official version of record. They are citable by the Digital Object Identifier (DOI®). “Just Accepted” is an optional service offered to authors. Therefore, the “Just Accepted” Web site may not include all articles that will be published in the journal. After a manuscript is technically edited and formatted, it will be removed from the “Just Accepted” Web site and published as an ASAP article. Note that technical editing may introduce minor changes to the manuscript text and/or graphics which could affect content, and all legal disclaimers and ethical guidelines that apply to the journal pertain. ACS cannot be held responsible for errors or consequences arising from the use of information contained in these “Just Accepted” manuscripts.

Hot Carrier and Surface Recombination Dynamics in Layered InSe Crystals

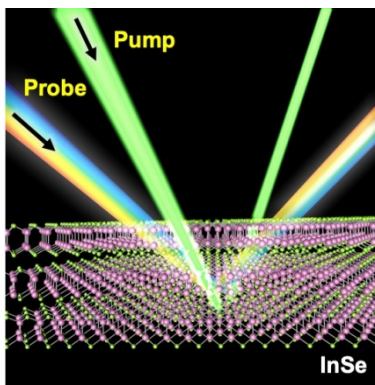
Chengmei Zhong,^{1,2} Vinod K. Sangwan,¹ Joohoon Kang,¹ Jan Luxa,³ Zdeněk Sofer,³ Mark C. Hersam,^{1,2,*} and Emily A. Weiss^{1,2,*}

1. *Department of Materials Science and Engineering, Northwestern University, Evanston, IL 60208*

2. *Department of Chemistry, Northwestern University, Evanston, IL 60208*

3. *Department of Inorganic Chemistry, University of Chemistry and Technology Prague Prague 6, Czech Republic*

*Corresponding authors: e-weiss@northwestern.edu; m-hersam@northwestern.edu



Abstract: Layered indium selenide (InSe) is a van der Waals solid that has emerged as a promising material for high-performance ultrathin solar cells. The optoelectronic parameters that are critical to photoconversion efficiencies, such as hot carrier lifetime and surface recombination velocity, are however largely unexplored in InSe. Here, these key photophysical properties of layered InSe are measured with femtosecond transient reflection spectroscopy. The hot carrier cooling process is found to occur through phonon scattering. The surface recombination velocity and ambipolar diffusion coefficient are extracted from fits to the pump energy-dependent transient reflection kinetics using a free carrier diffusion model. The extracted surface recombination velocity is approximately an order of magnitude larger than that for methylammonium lead-iodide perovskites, suggesting that surface recombination is a principal source of photocarrier loss in

1
2
3 InSe. The extracted ambipolar diffusion coefficient is consistent with previously reported values
4
5 of InSe carrier mobility.
6
7
8

9 **Keywords:** Layered indium selenide, van der Waals solid, solar cell, hot carrier dynamics,
10
11 transient reflection spectroscopy, surface recombination velocity, ambipolar diffusion coefficient
12
13
14
15
16
17
18
19
20
21
22
23
24
25
26
27
28
29
30
31
32
33
34
35
36
37
38
39
40
41
42
43
44
45
46
47
48
49
50
51
52
53
54
55
56
57
58
59
60

1
2
3 Layered indium selenide (InSe) has been aggressively investigated for high-performance
4 electronic and optoelectronics devices due to its high electron mobility and direct semiconducting
5 band gap at all thicknesses greater than three layers.¹⁻¹⁵ Since the band gap of multilayer InSe is
6 well-matched to the optimal Shockley-Queisser band gap, it is particularly promising for
7 photovoltaic applications. InSe also possesses low thermal conductivity (due to weak electron-
8 phonon coupling)¹⁶, which, in lead-iodide perovskites,¹⁷ leads to long hot carrier lifetimes (~100
9 ps) for a portion of the population; this slow thermalization could enable hot carriers to contribute
10 to the photocurrent and photovoltage within an InSe-based solar cell.¹⁸ Hot carrier solar cells are
11 theoretically predicted to have open circuit voltages larger than the band gaps of their component
12 semiconductors,¹⁹⁻²⁰ and, in principle, can operate above the Shockley-Queisser limit.²¹ Layered
13 bulk InSe was discovered over half a century ago²² and was subsequently studied as an absorbing
14 layer in Schottky solar cells with power conversion efficiencies exceeding 10%.²³⁻²⁶ As a van der
15 Waals solid, InSe has recently attracted renewed interest since exfoliation methods have shown
16 that ultrathin flakes of InSe are promising two-dimensional (2D) semiconductors for application
17 in ultrathin solar cells.²⁷⁻²⁹ The fabrication of high-performance photovoltaic junctions with
18 ultrathin active layers, however, requires minimization of non-radiative surface recombination,
19 which, in turn, requires fundamental studies of the surface recombination velocity (SRV).⁶

20
21 Here, we report the ultrafast hot carrier dynamics and surface recombination in layered InSe
22 crystals using broadband femtosecond transient reflection (TR) spectroscopy, as a function of
23 excited carrier density and excitation energy. These measurements yield three key findings: i) the
24 dependence of hot carrier dynamics in layered InSe crystals on the density of excited carriers is
25 similar to that in lead-iodide perovskite materials, in which phonon scattering mediates cooling;
26 ii) the ambipolar diffusion coefficient is $15.1 \text{ cm}^2\text{s}^{-1}$, consistent with previously reported values of
27
28
29
30
31
32
33
34
35
36
37
38
39
40
41
42
43
44
45
46
47
48
49
50
51
52
53
54
55
56
57
58
59
60

1
2
3 InSe carrier mobility; and (iii) the SRV is $4.1 \times 10^4 \text{ cm s}^{-1}$, smaller than that for unpassivated Si or
4 GaAs, but larger than that for methylammonium lead-iodide perovskites.³⁰⁻³¹ We expect that the
5 conclusions we present here for bulk layered InSe will be useful in characterizing carrier diffusion
6 and surface recombination in ultrathin flakes of InSe, where surface-mediated processes have even
7 more critical influence on device performance. With, for instance, transient absorption
8 microscopy³²⁻³³ the thickness dependence of these critical parameters could be extended to the 2D
9 limit.

10
11 Layered InSe crystals were grown by the Bridgman method; the details are described in the
12 Methods section (see Supporting Figures S1 and S2 for materials characterization).⁷ TR
13 spectroscopy was conducted on the InSe crystals, which were held in N₂ filled quartz cuvette to
14 avoid ambient degradation (see Methods). In general, for direct band gap semiconductors similar
15 to InSe, the refractive index is a factor of 5 to 20 larger than the extinction coefficient at most
16 visible wavelengths.³⁴ Thus, unlike the more commonly acquired transient absorption (TA)
17 spectrum, the intensities of features within the TR spectrum of bulk semiconductors are
18 approximately proportional to the pump photon-induced changes in refractive index, rather than
19 the pump photon-induced changes in extinction coefficient,^{30-31, 34} and the positive and negative
20 features in TR spectra cannot be simply interpreted as photoinduced absorptions and ground state
21 bleaches, respectively. Figure 1A (black trace) shows the TR spectrum of a single crystal of InSe
22 at 1 ps after pumping at 1.38 eV (bandgap ~ 1.25 eV). To correctly assign the features in the TR
23 spectrum, we convert it to the corresponding TA spectrum using an inverse Hilbert transformation
24 (iHT, or Kramers-Kronig transformation³⁰), Figure 1A (red trace). The validity of the iHT process
25 for obtaining TA data is confirmed by comparing the iHT of the TR spectrum to a directly acquired
26
27
28
29
30
31
32
33
34
35
36
37
38
39
40
41
42
43
44
45
46
47
48
49
50
51
52
53
54
55
56
57
58
59
60

1
2
3 TA spectrum of thin InSe flakes (still bulk-like) exfoliated from the same batch of the crystal (see
4
5 Supporting Figure S3).
6

7
8 A comparison of the derived TA spectrum with the steady-state absorption spectra (Figure 1A,
9
10 dashed blue trace) of exfoliated InSe flakes indicates that the narrow negative bleach feature in the
11
12 TA spectrum at 2.42 eV, and the corresponding derivative-like feature in the TR spectrum, are
13
14 attributable to the B exciton peak of InSe, which is the transition from a deep valence band state
15
16 (VB2) to the conduction band-edge,¹ as shown in Figure 1B. Discrete and sharp peak features in
17
18 TA/TR spectra usually indicate exciton formation (free carrier absorption features are usually
19
20 broad and continuous); however, in the case of InSe, for which the exciton binding energy is only
21
22 $\sim 0.5 k_B T$ at room temperature,³⁵ these sharp features are instead caused by the state-filling effect
23
24 of free carriers. Specifically, existing free carriers force newly photoexcited carriers to occupy
25
26 increasingly higher energy states through Pauli exclusion. This state-filling creates hypsochromic
27
28 shifts in the absorption/reflection spectra, which then translate to first order derivative-like features
29
30 in TR spectra.³⁶⁻³⁷
31
32
33
34

35
36 Figures 2A,C show that, when InSe is pumped at 1.38 eV (near the bandgap) such that minimal
37
38 hot carriers are created, the shape of the TR spectrum is constant over the entire time window of
39
40 the TR measurement (3 ns). Figures 2B,D show that, after pumping the sample at 3.06 eV (~ 1.9
41
42 eV above the band gap), which generates significant hot carrier population, the relative intensities
43
44 of the positive and negative peaks in TR spectra evolve over time, on two distinct timescales
45
46 (Supporting Figure S4 shows the normalized TR spectra). Before 5 ps (Figures 2B,D), the negative
47
48 peak of the TR feature is significantly suppressed relative to the positive peak due to the additional
49
50 TR contribution from hot carrier states. At a delay of ~ 5 ps, the excitonic features appear similar
51
52 to those in the spectrum of InSe pumped at 1.38 eV, indicating completion of the cooling process.
53
54
55
56
57
58
59
60

1
2
3 The dynamics of thermalization are most easily followed at probe photon energies (E_{probe}) near 2.5
4 eV, where the hot carrier contribution to the TR spectrum is maximized. Figure 3A shows kinetic
5 traces for hot carrier cooling, isolated by subtracting the early timescale (< 6 ps) TR kinetic trace
6 obtained with $E_{\text{pump}} = 1.38$ eV from the TR kinetic traces obtained with $E_{\text{pump}} = 3.06$ eV, 2.06 eV,
7 or 1.77 eV at the same excited carrier density (see the raw TR kinetics at $E_{\text{probe}} = 2.5$ eV in
8 Supporting Figure S6A). For an excited carrier density of $N_{\text{pump}} = 5 \times 10^{18} \text{ cm}^{-3}$, we measure hot
9 carrier cooling times of 0.61 – 0.99 ps (see the legend of Figure 3A), and no discernible dependence
10 of the cooling time on the energy of the pump photons.
11
12
13
14
15
16
17
18
19
20

21 Figures 3B,C show the dependence of the relaxation dynamics of hot carriers created with
22 $E_{\text{pump}} = 3.06$ eV as a function of N_{pump} (see the raw TR kinetics at $E_{\text{probe}} = 2.5$ eV in Supporting
23 Figure S6B). The lifetime for hot carrier cooling increases with increasing N_{pump} above a threshold
24 density of $\sim 10^{19} \text{ cm}^{-3}$, consistent with a hot-phonon bottleneck model. In this model, a higher hot
25 carrier density results in an increased population of non-equilibrium phonons, which increases the
26 chances of phonon reabsorption by thermalized free carriers and consequently reduces the net
27 carrier thermalization rate.³⁶ The cooling times of hot electrons in InSe single crystals extracted
28 from these data ($\sim 1 - 3.5$ ps) are comparable to the reported values in methylammonium lead-
29 iodide perovskites under similar excitation densities.^{32, 36} and significantly slower than those for
30 bulk Si³⁸ or GaAs³⁹. This result is reasonable since the large mass ratio of anion-to-cation in both
31 of these materials ($\sim 1.4:1$ for $\text{In}^{2+}:\text{Se}^{2-}$ and $\sim 2:1$ for $\text{Pb}^{2+}:\text{I}^{-}$)³⁶ results in large phononic bandgaps
32 that slow hot carrier cooling.⁴⁰
33
34
35
36
37
38
39
40
41
42
43
44
45
46
47
48

49 At later times (*e.g.*, 100 ps), the overall TR signal for the B exciton is lower and some of the
50 asymmetry of the features in the TR spectrum returns (Figure 2B and Supporting Figure S5), but
51
52
53
54
55
56
57
58
59
60

1
2
3 we suspect these changes are due to longer-timescale surface recombination processes discussed
4
5 directly below.
6

7
8 Figures 4A,B show the free carriers dynamics in single crystal InSe at later times (between 6
9
10 ps and 3 ns), when thermalization of carriers is complete. An E_{probe} of 2.38 eV and E_{pump} of 1.77
11
12 eV were chosen because, with these parameters, the TR spectra have maximum signal-to-noise
13
14 ratio and the TR intensity has a linear dependence on N_{pump} (see Supporting Figure S7). According
15
16 to a state-filling model,^{30, 37} such a linear dependence is a strong indication that the TR signal is
17
18 predominantly coming from free carriers, which are either free electrons in the lowest conduction
19
20 band level (CB) or free holes in a deep valence band level (VB2) shown in Figure 1B. The longer-
21
22 time (>6 ps) dynamics of recombination for free carriers in InSe are faster with higher E_{pump}
23
24 (Figure 4A), but the dependence of these dynamics on N_{pump} is negligible (Figure 4B). The fact
25
26 that free carrier dynamics have qualitatively different E_{pump} and N_{pump} dependencies at early times
27
28 (<6 ps) and later times (>6 ps) implies that they are governed by different mechanisms.
29
30
31
32

33 The free carrier dynamics of InSe after thermalization can be explained by a free carrier
34
35 diffusion model that includes surface recombination terms proposed by Yang *et al.*^{30-31, 41} Like
36
37 other bulk semiconductors,³⁰⁻³¹ the absorption coefficient of an InSe single crystal monotonically
38
39 increases with photon energy below 3.3 eV.²² Therefore, a pump pulse with higher E_{pump} leads to
40
41 a larger spatial gradient of the initial free carrier density near the sample surface, which produces
42
43 a larger carrier diffusion rate and faster surface recombination dynamics. The dynamics of the TR
44
45 signal are therefore sensitive to the pump energy because the TR measurement exclusively probes
46
47 carriers within ~20 nm of the semiconductor surface ($\lambda_{\text{probe}}/4\pi n$, where $\lambda_{\text{probe}} \equiv$ probe wavelength,
48
49 $n \equiv$ refractive index³⁰). We do not observe a dependence of free carrier dynamics on N_{pump} because
50
51
52
53
54
55
56
57
58
59
60

1
2
3 density-dependent bulk recombination of free carriers in inorganic semiconductors usually occurs
4
5 on timescales much larger than our measurement time window (>100 ns).^{30, 42}
6
7

8 Within the Yang model described above, the ambipolar diffusion coefficient D (i.e., the
9
10 average of electron and hole diffusion constants) and surface recombination velocities ($SRVs$)³⁰⁻
11
12 ^{31, 41} can be extracted by fitting the TR kinetic traces at $E_{\text{probe}} = 2.38$ eV between 6 ps and 3 ns with
13
14 equation 1:
15

$$\frac{\Delta R}{R}(t) = \frac{1}{SRV - \alpha D} [-\alpha D w(\alpha \sqrt{Dt}) + SRV w(SRV \sqrt{\frac{t}{D}})] \quad (1)$$

16
17
18
19
20 In equation 1, t is the pump-probe time delay, $w(x) = e^{x^2} \text{erfc}(x)$, and α is the absorption
21
22 coefficient of InSe at the corresponding pump photon energy: $\alpha = 5 \times 10^4 / 5 \times 10^3 / 1 \times 10^3 \text{ cm}^{-1}$ at
23
24 3.06/2.04/1.38 eV pump energies, respectively.²² We fit all of the kinetic traces in Figure 4A
25
26 simultaneously with equation 1 using a nonlinear least-squares global fitting routine where the
27
28 values of SRV and D are shared among all traces. We obtain an SRV value of $4.1 \times 10^4 \text{ cm s}^{-1}$, which
29
30 is approximately a factor of ten higher than that for methylammonium lead-iodide perovskite
31
32 materials,³¹ but a factor of 10 – 100 lower than those for inorganic bulk semiconductors used in
33
34 high efficiency solar cells (e.g., $SRV = 2.4 \times 10^5 \text{ cm s}^{-1}$ for unpassivated p-type Si⁴³, $SRV = 1.2 \times 10^6$
35
36 cm s^{-1} for n-type Si⁴³, $SRV = 8.5 \times 10^5 \text{ cm s}^{-1}$ for GaAs⁴⁴). This observation suggests that surface
37
38 recombination in InSe is at an intermediate level among common inorganic solar cell materials,
39
40 and partly explains why InSe solar cells only have moderate power conversion efficiencies despite
41
42 their excellent optical and electronic properties.²³⁻²⁴ Since the efficiency of Si and GaAs solar cells
43
44 improve greatly after surface passivation,⁴⁵⁻⁴⁶ it is reasonable to expect that similar improvements
45
46 can be achieved for InSe-based solar cells once a reliable surface passivation scheme is developed.
47
48
49
50
51

52 We extract a D value of $15.1 \text{ cm}^2 \text{ s}^{-1}$, which is also high compared to methylammonium lead-
53
54 iodide perovskites due to the higher carrier mobility of InSe. Using the Einstein relation $- \mu =$
55
56
57

1
2
3 $eD/k_B T$, where, e , k_B , and T are the electronic charge, the Boltzmann constant, and temperature,
4
5 respectively – we estimate the average photocarrier mobility (μ) near the surface of InSe to be
6
7 $\sim 500 \text{ cm}^2 \text{V}^{-1} \text{s}^{-1}$. This value is similar to the highest reported values of intralayer electron and hole
8
9 mobilities at room temperature in single crystal InSe ($\sim 1000 \text{ cm}^2 \text{V}^{-1} \text{s}^{-1}$ for electrons,^{1,3,5} $\sim 30 \text{ cm}^2 \text{V}^{-1}$
10
11 s^{-1} for holes⁴⁷). The low mobility value we measure (relative to published values) is possibly
12
13 attributable to the fact that the TR measurement is performed at an oblique reflection angle, which
14
15 causes our estimate to be the average of interlayer mobility ($10^{-1} \sim 10^0 \text{ cm}^2 \text{V}^{-1} \text{s}^{-1}$)⁴⁸ and intralayer
16
17 mobility ($\sim 10^3 \text{ cm}^2 \text{V}^{-1} \text{s}^{-1}$).

18
19
20
21 In conclusion, we have studied the hot carrier and surface recombination dynamics of InSe
22
23 single crystals with femtosecond transient reflection (TR) spectroscopy. The hot carrier lifetime is
24
25 dependent on excited carrier density, indicating that the cooling process is caused by phonon
26
27 scattering. The relatively long hot carrier lifetime ($\sim 1 \text{ ps}$ for a carrier density of 10^{18} cm^{-3}) is likely
28
29 caused by the large phononic band gap created by the large mass ratio between anion (In^{2+}) and
30
31 cation (Se^{2-}). We further determined the values of critical parameters for solar cell device
32
33 engineering, specifically the ambipolar diffusion coefficient (D) and the surface recombination
34
35 velocity (SRV), by modeling the dynamics of free carriers after they have thermalized ($>6 \text{ ps}$) using
36
37 drift-diffusion equations that include surface recombination.³⁰⁻³¹ The measured ambipolar
38
39 diffusion constant D is $15.1 \text{ cm}^2 \text{s}^{-1}$, which is consistent with published values of carrier mobility
40
41 in InSe. Our extracted SRV value of $4.1 \times 10^4 \text{ cm s}^{-1}$ is at an intermediate level among common
42
43 inorganic solar cell materials, and suggests that the development of surface passivation schemes
44
45 for InSe could minimize surface recombination and improve power conversion efficiencies. An
46
47 additional question is whether there is any impact on the observed hot carrier dynamics due to
48
49 depopulation of VB2 into VB1. In principle, it is possible to combine the TR spectra and kinetics
50
51
52
53
54
55
56
57
58
59
60

1
2
3 of the A-exciton regions in the near-infrared with the visible-region TR data to decouple the VB2-
4 to-VB1 transition from hot carrier dynamics. In practice, however, the much lower signal-to-noise
5 and time-dependent peak shifts in the NIR data prevent us from doing so here; some further
6 experimental optimization is warranted to pursue this issue. Overall, this work reveals the key
7 photophysical properties of InSe, which will inform ongoing efforts to realize high-performance
8 optoelectronic and photovoltaic applications based on this emerging van der Waals solid.
9
10
11
12
13
14
15
16
17
18

19 **METHODS**

20
21 **InSe Single Crystal Growth and TR Sample Preparation.** InSe crystal growth is described
22 elsewhere.⁷ Detailed structural characterization of InSe single crystals are given in the Supporting
23 Information (Figures S1 and S2). For TR measurements, small pieces of atomically flat InSe
24 crystals with surface areas $>0.1 \text{ cm}^2$ and thicknesses $>0.1 \text{ mm}$ were cleaved perpendicular to the
25 surface normal from the InSe crystal ingot by a pair of tweezers inside a nitrogen glovebox.. The
26 small pieces were then taped onto glass substrates and deposited into quartz cuvettes, which were
27 sealed with Teflon tape and vacuum grease inside the glovebox before being taken into ambient
28 conditions for TR measurements.
29
30
31
32
33
34
35
36
37
38
39

40 **Transient Reflection Spectroscopy Measurements in the Visible Wavelength Region.**
41 Visible transient reflection spectroscopy measurements were performed following previously
42 published protocols⁴⁹⁻⁵⁰ with the addition of two silver mirrors before the probe detector to adjust
43 the beam path for reflection geometries. The inverse Hilbert transform of TR spectral data was
44 performed with the commercial module incorporated in OriginPro 8.6 (OriginLab).
45
46
47
48
49
50
51
52
53
54
55
56
57
58
59
60

FIGURES

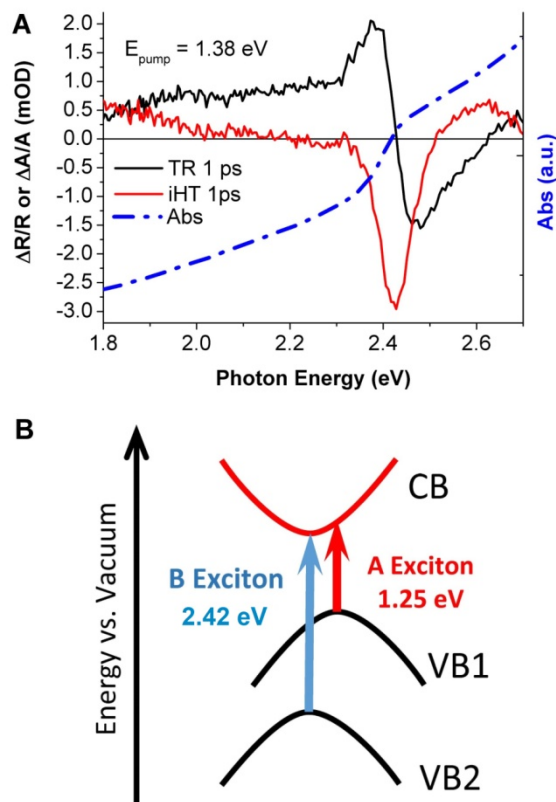


Figure 1. (A) TR spectrum of an InSe single crystal pumped at 1.38 eV photon energy (black), and the inverse Hilbert transform (iHT) of the TR spectrum (red), which represents the surface transient absorption spectrum through the Kramers–Kronig relationship. The dashed blue trace is the ground state absorption spectrum of an exfoliated thin film taken from the same batch of InSe crystals. (B) Schematic of electronic transitions in single crystal InSe corresponding to A and B exciton absorption peaks according to the theoretical calculations in Ref [1]. CB stands for the conduction band, VB1 and VB2 stand for the highest and the second highest valence bands, respectively. The derivative-like feature centered around 2.4 eV in the TR spectrum in (A) corresponds to a ground state bleach in the TA spectrum, with an energy that matches the transition from VB2 to CB in (B). The broad positive feature from 1.8 eV to 2.2 eV in the TR spectrum in (A) is a photoinduced absorption feature (probably due to free carrier absorptions in InSe) in the TA spectrum.

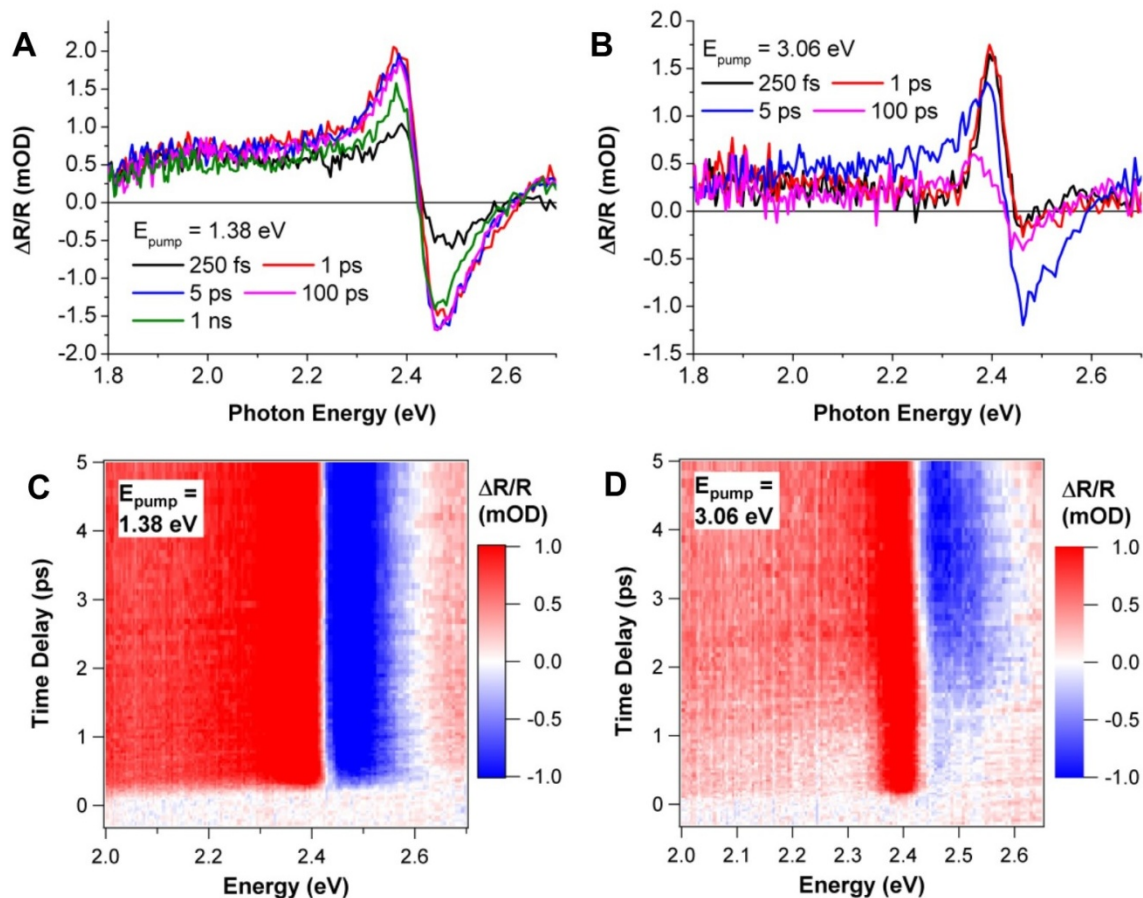


Figure 2. (A, B) TR spectra of an InSe single crystal in the visible region, at time delays of 250 fs, 1 ps, 5 ps, and 100 ps after excitation at 1.38 eV pump energy (near the bandgap, A) and 3.06 eV pump energy (1.9 eV above the bandgap, B), respectively. (C, D) Pseudo-color 2D images of TR spectra of an InSe single crystal pumped at 1.38 eV (C) or 3.06 eV (D). The horizontal axis is the probe photon energy (eV), and the vertical axis is the pump-probe time delay (ps). The color intensity indicated by the scale bar represents the TR intensity (mOD).

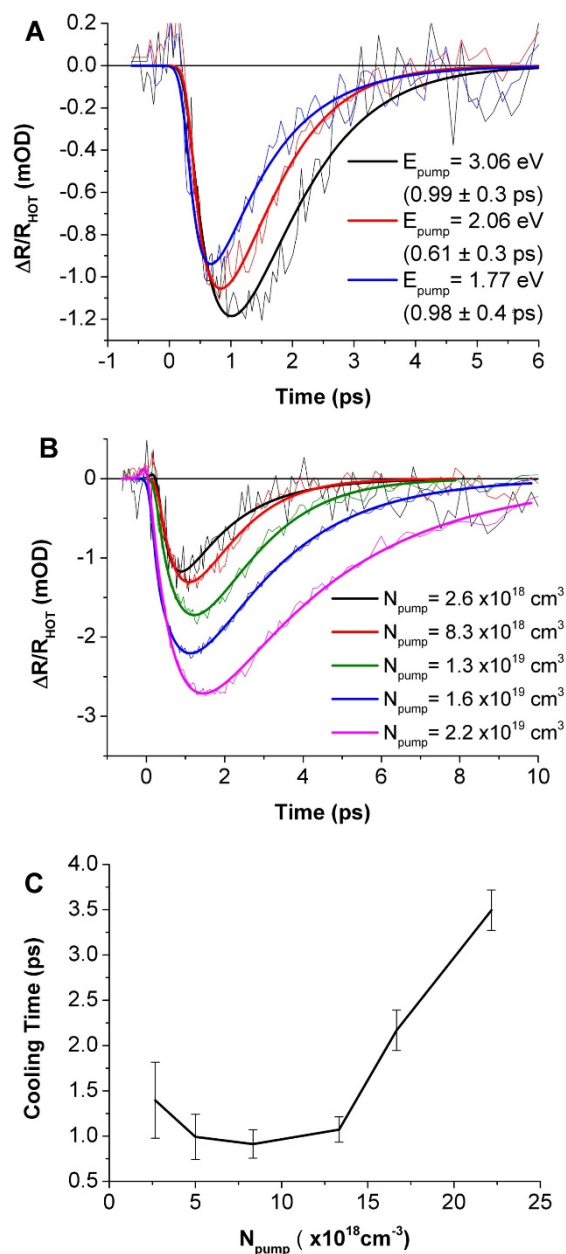


Figure 3. (A) Hot carrier thermalization dynamics of single crystal InSe extracted from Figure S4A by subtracting the raw TR kinetic trace acquired at $E_{\text{pump}} = 1.38 \text{ eV}$ from the kinetic traces acquired at $E_{\text{pump}} = 3.06 \text{ eV}$, 2.06 eV , or 1.77 eV , as indicated. The cooling times from exponential fits of the kinetic traces are shown in the legend. N_{pump} is fixed at $5 \times 10^{18} \text{ cm}^{-3}$ for all pump energies. (B) Hot carrier thermalization dynamics of single crystal InSe extracted from Figure S4B for $E_{\text{pump}} = 3.06 \text{ eV}$, with $N_{\text{pump}} = 2.6, 5, 8.3, 13, 16,$ or $22 \times 10^{18} \text{ cm}^{-3}$, respectively. The corresponding thermalization lifetimes are plotted vs. N_{pump} in (C).

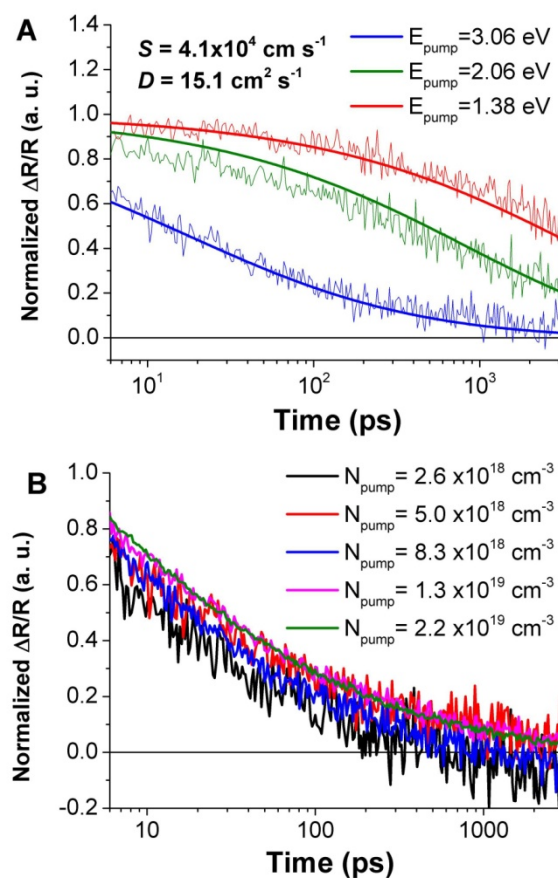


Figure 4. (A) E_{pump} dependent TR kinetic traces (normalized at their peak values at ~ 2 ps) from 6 ps to 3 ns of an InSe single crystal, pumped at 2.38 eV from the TR spectrum of the same InSe crystal, and pumped with a fixed N_{pump} of $5 \times 10^{18} \text{ cm}^{-3}$; the nonlinear least-squares global best-fit curves from 6 ps to 3 ns using equation 1 and the extracted values of SRV (S) and diffusion constant (D), are shown. (B) N_{pump} dependent normalized TR kinetic traces (normalized at a maximum at ~ 2 ps) from 6 ps to 3 ns extracted at $E_{\text{probe}} = 2.38$ eV probe energy and $E_{\text{pump}} = 3.06$ eV.

SUPPORTING INFORMATION

TEM and XRD characterizations of InSe single crystal samples; additional transient reflection spectroscopy data and analysis; and Figures S1-S7.

ACKNOWLEDGMENTS

This research was supported by the Materials Research Science and Engineering Center (MRSEC) of Northwestern University (NSF DMR-1720139) (spectroscopy) and the Center for Light Energy Activated Redox Processes (LEAP), an Energy Frontier Research Center funded by the U. S. Department of Energy, Office of Science, Basic Energy Sciences under Award No. DE-SC0001059 (sample preparation and characterization). Z. S. and J. L. were supported by the Czech Science Foundation (GACR No. 17-11456S), Neuron Foundation for scientific support and by the project Advanced Functional Nanorobots (reg. No. CZ.02.1.01/0.0/0.0/15_003/0000444 financed by the EFRR).

REFERENCES

- (1) Bandurin, D. A.; Tyurnina, A. V.; Yu, G. L.; Mishchenko, A.; Zólyomi, V.; Morozov, S. V.; Kumar, R. K.; Gorbachev, R. V.; Kudrynskiy, Z. R.; Pezzini, S.; Kovalyuk, Z. D.; Zeitler, U.; Novoselov, K. S.; Patanè, A.; Eaves, L.; Grigorieva, I. V.; Fal'ko, V. I.; Geim, A. K.; Cao, Y. High electron mobility, quantum Hall effect and anomalous optical response in atomically thin InSe. *Nat. Nanotech.* **2016**, *12*, 223.
- (2) Yang, Z.; Jie, W.; Mak, C.-H.; Lin, S.; Lin, H.; Yang, X.; Yan, F.; Lau, S. P.; Hao, J. Wafer-Scale Synthesis of High-Quality Semiconducting Two-Dimensional Layered InSe with Broadband Photoresponse. *ACS Nano* **2017**, *11*, 4225-4236.
- (3) Ho, P.-H.; Chang, Y.-R.; Chu, Y.-C.; Li, M.-K.; Tsai, C.-A.; Wang, W.-H.; Ho, C.-H.; Chen, C.-W.; Chiu, P.-W. High-Mobility InSe Transistors: The Role of Surface Oxides. *ACS Nano* **2017**, *11*, 7362-7370.

- 1
2
3 (4) Lei, S. D.; Ge, L. H.; Najmaei, S.; George, A.; Kappera, R.; Lou, J.; Chhowalla, M.;
4 Yamaguchi, H.; Gupta, G.; Vajtai, R.; Mohite, A. D.; Ajayan, P. M. Evolution of the electronic
5 band structure and efficient photo-detection in atomic layers of InSe. *ACS Nano* **2014**, *8*, 1263-
6 1272.
7
8
9
10 (5) Li, M.; Lin, C.-Y.; Yang, S.-H.; Chang, Y.-M.; Chang, J.-K.; Yang, F.-S.; Zhong, C.; Jian,
11 W.-B.; Lien, C.-H.; Ho, C.-H.; Liu, H.-J.; Huang, R.; Li, W.; Lin, Y.-F.; Chu, J. High Mobilities
12 in Layered InSe Transistors with Indium-Encapsulation-Induced Surface Charge Doping. *Adv.*
13 *Mater.* **2018**, *0*, 1803690.
14
15
16
17 (6) Nelson, J. *The Physics of Solar Cells*. Imperial College Press: 2003.
18
19 (7) Kang, J.; Wells, S. A.; Sangwan, V. K.; Lam, D.; Liu, X.; Luxa, J.; Sofer, Z.; Hersam, M.
20 C. Solution-Based Processing of Optoelectronically Active Indium Selenide. *Adv. Mater.* **2018**,
21 *30*, 1802990.
22
23
24 (8) Sangwan, V. K.; Hersam, M. C. Electronic Transport in Two-Dimensional Materials.
25 *Annual Rev. Phys. Chem.* **2018**, *69*, 299-325.
26
27 (9) Kang, J.; Sangwan, V. K.; Lee, H.-S.; Liu, X.; Hersam, M. C. Solution-Processed Layered
28 Gallium Telluride Thin-Film Photodetectors. *ACS Photon.* **2018**, *5*, 3996-4002.
29
30 (10) Sucharitakul, S.; Goble, N. J.; Kumar, U. R.; Sankar, R.; Bogorad, Z. A.; Chou, F.-C.; Chen,
31 Y.-T.; Gao, X. P. A. Intrinsic Electron Mobility Exceeding $10^3 \text{ cm}^2/(\text{V s})$ in Multilayer InSe FETs.
32 *Nano Lett.* **2015**, *15*, 3815-3819.
33
34
35 (11) Mudd, G. W.; Svatek, S. A.; Hague, L.; Makarovskiy, O.; Kudrynskiy, Z. R.; Mellor, C. J.;
36 Beton, P. H.; Eaves, L.; Novoselov, K. S.; Kovalyuk, Z. D.; Vdovin, E. E.; Marsden, A. J.; Wilson,
37 N. R.; Patanè, A. High Broad-Band Photoresponsivity of Mechanically Formed InSe–Graphene
38 van der Waals Heterostructures. *Adv. Mater.* **2015**, *27*, 3760-3766.
39
40 (12) Lei, S.; Wen, F.; Ge, L.; Najmaei, S.; George, A.; Gong, Y.; Gao, W.; Jin, Z.; Li, B.; Lou,
41 J.; Kono, J.; Vajtai, R.; Ajayan, P.; Halas, N. J. An Atomically Layered InSe Avalanche
42 Photodetector. *Nano Lett.* **2015**, *15*, 3048-3055.
43
44 (13) Tamalampudi, S. R.; Lu, Y.-Y.; Kumar, U. R.; Sankar, R.; Liao, C.-D.; Moorthy, B. K.;
45 Cheng, C.-H.; Chou, F. C.; Chen, Y.-T. High Performance and Bendable Few-Layered InSe
46 Photodetectors with Broad Spectral Response. *Nano Lett.* **2014**, *14*, 2800-2806.
47
48 (14) Hamer, M.; Tóvári, E.; Zhu, M.; Thompson, M. D.; Mayorov, A.; Prance, J.; Lee, Y.; Haley,
49 R. P.; Kudrynskiy, Z. R.; Patanè, A.; Terry, D.; Kovalyuk, Z. D.; Ensslin, K.; Kretinin, A. V.;
50
51
52
53
54
55
56
57
58
59
60

1
2
3 Geim, A.; Gorbachev, R. Gate-Defined Quantum Confinement in InSe-Based van der Waals
4 Heterostructures. *Nano Lett.* **2018**, *18*, 3950-3955.

5
6 (15) Premasiri, K.; Radha, S. K.; Sucharitakul, S.; Kumar, U. R.; Sankar, R.; Chou, F.-C.; Chen,
7 Y.-T.; Gao, X. P. A. Tuning Rashba Spin–Orbit Coupling in Gated Multilayer InSe. *Nano Lett.*
8 **2018**, *18*, 4403-4408.

9
10 (16) Indium selenide (InSe) electrical and thermal conductivity. In *Non-Tetrahedrally Bonded*
11 *Elements and Binary Compounds I*, Madelung, O.; Rössler, U.; Schulz, M., Eds. Springer Berlin
12 Heidelberg: Berlin, Heidelberg, 1998; Vol. 41C, pp 1-5.

13
14 (17) Frost, J. M.; Whalley, L. D.; Walsh, A. Slow Cooling of Hot Polarons in Halide Perovskite
15 Solar Cells. *ACS Energy Lett.* **2017**, *2*, 2647-2652.

16
17 (18) Yang, J.; Wen, X.; Xia, H.; Sheng, R.; Ma, Q.; Kim, J.; Tapping, P.; Harada, T.; Kee, T.
18 W.; Huang, F.; Cheng, Y.-B.; Green, M.; Ho-Baillie, A.; Huang, S.; Shrestha, S.; Patterson, R.;
19 Conibeer, G. Acoustic-optical phonon up-conversion and hot-phonon bottleneck in lead-halide
20 perovskites. *Nat. Commun.* **2017**, *8*, 14120.

21
22 (19) Ross, R. T.; Nozik, A. J. Efficiency of hot-carrier solar energy converters. *J. Appl. Phys.*
23 **1982**, *53*, 3813-3818.

24
25 (20) Würfel, P. Solar energy conversion with hot electrons from impact ionisation. *Sol. Energy*
26 *Mater. Sol. Cells* **1997**, *46*, 43-52.

27
28 (21) Nozik, A. J. Spectroscopy and Hot Electron Relaxation Dynamics in Semiconductor
29 Quantum Wells and Quantum Dots. *Annual Rev. Phys. Chem.* **2001**, *52*, 193-231.

30
31 (22) Damon, R. W.; Redington, R. W. Electrical and Optical Properties of Indium Selenide.
32 *Phys. Rev.* **1954**, *96*, 1498-1500.

33
34 (23) Martínez-Pastor, J.; Segura, A.; Valdés, J. L.; Chevy, A. Electrical and photovoltaic
35 properties of indium-tin-oxide/p-InSe/Au solar cells. *J. Appl. Phys.* **1987**, *62*, 1477-1483.

36
37 (24) Segura, A.; Chevy, A.; Guesdon, J. P.; Besson, J. M. Photovoltaic efficiency of InSe solar
38 cells. *Sol. Energy Mater.* **1979**, *2*, 159-165.

39
40 (25) Gnatenko, Y. P.; Zhirko, Y. I. Exciton Absorption and Luminescence of Indium Selenide
41 Crystals. *physica status solidi (b)* **1987**, *142*, 595-604.

42
43 (26) Williams, R. H.; McCanny, J. V.; Murray, R. B.; Ley, L.; Kemeny, P. C. The electronic
44 band structure of indium selenide: photoemission and theory. *J. Phys. C: Solid State Phys.* **1977**,
45 *10*, 1223.

- 1
2
3 (27) Wong, J.; Jariwala, D.; Tagliabue, G.; Tat, K.; Davoyan, A. R.; Sherrott, M. C.; Atwater,
4 H. A. High Photovoltaic Quantum Efficiency in Ultrathin van der Waals Heterostructures. *ACS*
5 *Nano* **2017**, *11*, 7230-7240.
6
7
8 (28) Atwater, H. A.; Davoyan, A. R.; Ilic, O.; Jariwala, D.; Sherrott, M. C.; Went, C. M.;
9 Whitney, W. S.; Wong, J. Materials challenges for the Starshot lightsail. *Nat. Mater.* **2018**, *17*,
10 861-867.
11
12
13 (29) Jariwala, D.; Davoyan, A. R.; Wong, J.; Atwater, H. A. Van der Waals Materials for
14 Atomically-Thin Photovoltaics: Promise and Outlook. *ACS Photon.* **2017**, *4*, 2962-2970.
15
16
17 (30) Yang, Y.; Yan, Y.; Yang, M.; Choi, S.; Zhu, K.; Luther, J. M.; Beard, M. C. Low surface
18 recombination velocity in solution-grown CH₃NH₃PbBr₃ perovskite single crystal. *Nat. Commun.*
19 **2015**, *6*, 7961.
20
21
22 (31) Yang, Y.; Yang, M.; Moore, David T.; Yan, Y.; Miller, Elisa M.; Zhu, K.; Beard,
23 Matthew C. Top and bottom surfaces limit carrier lifetime in lead iodide perovskite films. *Nat.*
24 *Energy* **2017**, *2*, 16207.
25
26
27 (32) Guo, Z.; Wan, Y.; Yang, M.; Snaider, J.; Zhu, K.; Huang, L. Long-range hot-carrier
28 transport in hybrid perovskites visualized by ultrafast microscopy. *Science* **2017**, *356*, 59-62.
29
30
31 (33) Nah, S.; Spokoyny, B.; Stoumpos, C.; Soe, C. M. M.; Kanatzidis, M.; Harel, E. Spatially
32 segregated free-carrier and exciton populations in individual lead halide perovskite grains. *Nat.*
33 *Photon.* **2017**, *11*, 285.
34
35
36 (34) Yu, P. Y.; Cardona, M. *Fundamentals of Semiconductors*. Springer-Verlag: New York,
37 1996.
38
39 (35) Camassel, J.; Merle, P.; Mathieu, H.; Chevy, A. Excitonic absorption edge of indium
40 selenide. *Phys. Rev. B* **1978**, *17*, 4718-4725.
41
42
43 (36) Yang, Y.; Ostrowski, D. P.; France, R. M.; Zhu, K.; van de Lagemaat, J.; Luther, J. M.;
44 Beard, M. C. Observation of a hot-phonon bottleneck in lead-iodide perovskites. *Nat. Photon.*
45 **2015**, *10*, 53.
46
47
48 (37) Huang, D.; Chyi, J.-I.; Morkoç, H. Carrier effects on the excitonic absorption in GaAs
49 quantum-well structures: Phase-space filling. *Phys. Rev. B* **1990**, *42*, 5147-5153.
50
51 (38) Goldman, J. R.; Prybyla, J. A. Ultrafast dynamics of laser-excited electron distributions in
52 silicon. *Phys. Rev. Lett.* **1994**, *72*, 1364-1367.
53
54
55
56
57
58
59
60

- 1
2
3 (39) Elsaesser, T.; Shah, J.; Rota, L.; Lugli, P. Initial thermalization of photoexcited carriers in
4 GaAs studied by femtosecond luminescence spectroscopy. *Phys. Rev. Lett.* **1991**, *66*, 1757-1760.
5
6 (40) Conibeer, G.; Shrestha, S.; Huang, S.; Patterson, R.; Xia, H.; Feng, Y.; Zhang, P.; Gupta,
7 N.; Tayebjee, M.; Smyth, S.; Liao, Y.; Zhang, Z.; Chung, S.; Lin, S.; Wang, P.; Dai, X. In *Hot*
8 *carrier solar cell absorbers: materials, mechanisms and nanostructures*, SPIE Solar Energy +
9 Technology, SPIE: 2014; p 11.
10
11 (41) Tanaka, T.; Harata, A.; Sawada, T. Subpicosecond surface-restricted carrier and thermal
12 dynamics by transient reflectivity measurements. *J. Appl. Phys.* **1997**, *82*, 4033-4038.
13
14 (42) Yamada, Y.; Nakamura, T.; Endo, M.; Wakamiya, A.; Kanemitsu, Y. Photocarrier
15 Recombination Dynamics in Perovskite CH₃NH₃PbI₃ for Solar Cell Applications. *J. Am. Chem.*
16 *Soc.* **2014**, *136*, 11610-11613.
17
18 (43) Sabbah, A. J.; Riffe, D. M. Measurement of silicon surface recombination velocity using
19 ultrafast pump-probe reflectivity in the near infrared. *J. Appl. Phys.* **2000**, *88*, 6954-6956.
20
21 (44) Beard, M. C.; Turner, G. M.; Schmittenmaer, C. A. Transient photoconductivity in GaAs
22 as measured by time-resolved terahertz spectroscopy. *Phys. Rev. B* **2000**, *62*, 15764-15777.
23
24 (45) Aberle, A. G. Surface passivation of crystalline silicon solar cells: a review. *Prog.*
25 *Photovolt: Res. Appl.* **2000**, *8*, 473-487.
26
27 (46) Mauk, M. G.; Xu, S.; Arent, D. J.; Mertens, R. P.; Borghs, G. Study of novel chemical
28 surface passivation techniques on GaAs pn junction solar cells. *Appl. Phys. Lett.* **1989**, *54*, 213-
29 215.
30
31 (47) Segura, A.; Pomer, F.; Cantarero, A.; Krause, W.; Chevy, A. Electron scattering
32 mechanisms in n-type indium selenide. *Phys. Rev. B* **1984**, *29*, 5708-5717.
33
34 (48) Segura, A.; Guesdon, J. P.; Besson, J. M.; Chevy, A. Photoconductivity and photovoltaic
35 effect in indium selenide. *J. Appl. Phys.* **1983**, *54*, 876-888.
36
37 (49) Bettis Homan, S.; Sangwan, V. K.; Balla, I.; Bergeron, H.; Weiss, E. A.; Hersam, M. C.
38 Ultrafast Exciton Dissociation and Long-Lived Charge Separation in a Photovoltaic Pentacene-
39 MoS₂ van der Waals Heterojunction. *Nano Lett.* **2017**, *17*, 164-169.
40
41 (50) Zhong, C.; Sangwan, V. K.; Wang, C.; Bergeron, H.; Hersam, M. C.; Weiss, E. A.
42 Mechanisms of Ultrafast Charge Separation in a PTB7/Monolayer MoS₂ van der Waals
43 Heterojunction. *J. Phys. Chem. Lett.* **2018**, *9*, 2484-2491.
44
45
46
47
48
49
50
51
52
53
54
55
56
57
58
59
60